IEEE Robotics and Automation Letters (RA-L) paper, presented at ICRA 2026, Vienna, Austria. Cite as RA-L paper.

Passive Adaptive Object Prehension, Retention, and Release with a Mechanically Intelligent Gripper

Ming Chun CHAN†, Jiayun LI† , Ziyao WU, Nan WANG, and Rob B.N. SCHARFF*

***Abstract*—This article presents a mechanically intelligent gripper that is capable of passive and adaptive object prehension, passive object retention, and passive object release. Passive adaptive prehension is achieved through a compliant linkage with two Fin Ray fingers that enclose an object when the gripper is pushed onto it. The object is held firmly in place during transport by a linear ratchet mechanism that locks the compliant mechanism in place. An asymmetric ratchet release mechanism releases the object using gravitational force when the gripper is maneuvered in its release-orientation. The absence of actuators, electronics, and a tether or embedded power source make the presented adaptive gripper a promising technology for challenging environments where low energy consumption and robustness to dirt and water are critical.**

***Index Terms*—Compliant joints and mechanisms, embodied intelligence, underactuated robots.**

I. INTRODUCTION

A key challenge for dexterous robotic manipulation is the development of end effectors that can adaptively grasp objects of various shapes and sizes. Rigid grippers typically require large numbers of actuators and sensors to realize such adaptive behavior [1]. As a result, these grippers are often expensive, energy-inefficient, difficult to control, and lacking robustness for operation in extreme environments.

Soft robotic grippers [2] and rigid underactuated grippers [3]–[6] are capable of passively adapting to the shape of an object, thereby greatly reducing the required number of actuators and sensors for adaptive grasping. Zhai et al. further reduce the required number of actuators and sensors of a soft pneumatic gripper by embedding a fluidic control circuit that enables the gripper to pick up objects by pressing it onto an object and to release objects by tilting the gripper [7]. Other grippers include mechanisms to minimize energy consumption in the retention phase [8]–[13]. However, all of the aforementioned grippers still require at least one actuator for object prehension.

Fully passive grippers are designed with the intention to completely eliminate the need for actuators by leveraging the existing degrees of freedom (DOFs) of an external system such as a robotic arm, unmanned aerial vehicle (UAV) or unmanned underwater vehicle (UUV) to grasp, hold, and release an object. Hsiao et al. presented a passive gripper mounted on a UAV capable of prehension, retention, and release of an object using only the DOFs of the drone [14]. However, the gripper is not adaptive and limited to form closure of objects with holes. Moreover, release of the object requires contact with the ground, precluding its use for common pick and place tasks such as object sorting where the object has to be dropped inside a container, as well as mid-air or mid-water release with UAVs and UUVs. Hsiao et al. also presented a passive perching mechanism for quadcopters combining a bistable mechanism with a suction cup [15]. However, the mechanism still requires a servo motor to lock the mechanism. Lee et al. presented a passive mechanism for overhead perching with UAVs using a central rod coupled to adaptive Fin Ray fingers [16]. However, the UAV needs to produce continuous upward thrust to hold the support and the support has to be anchored to the ground to oppose this force. This makes it energy inefficient and unsuitable for pick-and-place applications where the object is not anchored to the ground but needs to be transported between locations. Nagaoka et al. presented a gripper that can passively grasp and hold objects, but deploy tendon-driven actuation to release the object [17]. Moreover, the rigid fingers limit the ability of the gripper to adapt to the shape of the object. A passive gripper inspired by the sea anemone was presented by Qi et al. [18]. A

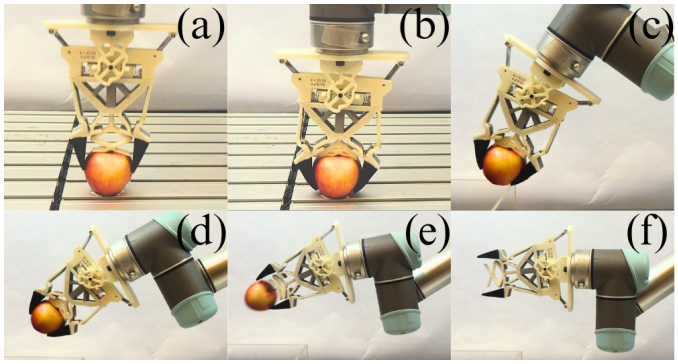

Fig. 1. Passive adaptive object prehension, retention, and releasing process: (a) preparation for contact, (b) the robot arm pushes the central rod onto the object which causes the Fin Ray fingers to rotate and secure the object, (c) object prehension completed and lift up, (d) retention of the object, (e) controlled release of the object using gravitational force by maneuvering the gripper in its release-orientation, (e) object release completed and ready for picking up the next object.

Manuscript received: May 22, 2025; Revised August 1, 2025; Accepted September 1, 2025.

This paper was recommended for publication by Editor Yong-Lae Park upon evaluation of the Associate Editor and Reviewers comments.

The authors are with the Division of Integrative Systems and Design, The Hong Kong University of Science and Technology, Clear Water Bay, Hong Kong. This work was supported by the "Sustainable Smart Campus as a Living Lab" (SSC) program at The Hong Kong University of Science and Technology (HKUST).

† These authors contributed equally to this work

* Corresponding Author (E-mail: scharffrbn@ust.hk)

Digital Object Identifier (DOI): see top of this page.

IEEE Robotics and Automation Letters (RA-L) paper, presented at ICRA 2026, Vienna, Austria. Cite as RA-L paper.

bistable structure with pins allows for contact-triggered passive adaptive prehension and passive retention of objects, but a positive pressure is required to make the bistable structure snap back to its original state in order to release the object. Finally, Nate et al. [19] present a passive gripper that can passively grasp, hold, and release an object using a locking mechanism. However, the grasping is limited to a caging grasp and it also requires contact with the ground to release the object.

Here, we present a passive gripper that is able to adaptively grasp, hold, and release objects, solely relying on the DOFs of an external system such as a robot arm (see Fig. 1). The contribution of this work is two-fold:

- The design, modeling, and experimental validation of a passive and contactless object release mechanism.
- The integration of passive prehension, retention, and release mechanisms to realize the first gripper capable of passive adaptive prehension, passive retention, and passive contactless release.

The gripper can be manufactured using low-cost materials and desktop 3D-printers. The presented gripper is a promising technology for deployment in challenging environments where low energy consumption, robustness to dirt and water, and low costs are critical.

II. PASSIVE GRIPPER MODELING & DESIGN

The passive gripper is illustrated in Fig. 1. It comprises two outward facing Fin Ray fingers that rotate inward when the central rod is pushed onto an object, thereby grasping the object. A linear ratchet mechanism secures the central rod and ensures the gripping force continues to be applied to the object upon lifting. Finally a gravity-based release mechanism releases the object when the gripper is rotated into its release orientation. The following subsections will discuss the design and modeling of the linkage, locking mechanism, and release mechanism. A nomenclature for the symbols used is these subsections is provided in Table I.

A. Linkage, Fin Ray fingers, and central rod tip

The central rod and Fin Ray fingers are coupled through a linkage with compliant joints, as illustrated in Fig. 2. The lengths of the links were chosen as $l_{\mathrm{ab}} = 53.5\mathrm{mm}$, $l_{\mathrm{bc}} = 20.5\mathrm{mm}$, $l_{\mathrm{cd}} = 15.2\mathrm{mm}$, $l_{\mathrm{ad}} = 52.0\mathrm{mm}$, and the length of the lever l_{ce} was chosen as 12.0 mm. To calculate the kinematics of the linkage, bar ad was set as the ground link and set as the x-axis of the coordinate system with point a being the origin (see Fig. 2(a)).

To find the relationship between the vertical displacement of the central rod Δh and the Fin Ray finger angle α (see Fig. 2(b)), the following relations were added:

$$
\begin{aligned}
a &= (0,0)\\
c &= (l_{\mathrm{ab}} + l_{\mathrm{bc}} \cdot \cos(\pi - \theta_2), l_{\mathrm{ab}} \cdot \sin(\pi - \theta_2))\\
b &= (l_{\mathrm{ad}} \cdot \cos(\theta_1), l_{\mathrm{ad}} \cdot \sin(\theta_1))\\
d &= (l_{\mathrm{ab}}, 0)\\
e &= (c_x + l_{\mathrm{ce}} \cos\theta_5, c_y + l_{\mathrm{ce}} \sin\theta_5)\\
\alpha &= \theta_7 + (\theta_8 - \theta_5)\\
\Delta h &= \Delta e_y + \tan\theta_6 \cdot \Delta e_x
\end{aligned}
$$

TABLE I
PASSIVE ADAPTIVE GRIPPER NOMENCLATURE

Symbol	Description
Linkage	
a, b, c, d, e	Linkage joints and endpoint
$l_{\mathrm{ab}}, l_{\mathrm{bc}}, l_{\mathrm{cd}}, l_{\mathrm{ad}}, l_{\mathrm{ce}}$	Lengths of the linkage bars
$\theta_1, \theta_2, \theta_3, \theta_4, \theta_5, \theta_6, \theta_7, \theta_8$	Joint angles of the linkage and angular offsets
α	Fin Ray finger angle
Δh	Vertical displacement of the central rod
l_{f}	The gripper opening
Locking mechanism	
μ	Friction coefficient between the pawl surface and tooth surface
γ	Friction angle between pawl and teeth on the central rod
β	Angle of the locking pin
k_{l}	Spring constant of the pawl springs
F_{s}	Pawl spring force
F_{n}	Normal reaction force
F_{p}	Pushing force required to lift the rod
F_{f}	Friction force between pawl and teeth on the central rod
F_{r}	Resultant force from the normal reaction force and friction force
w_{t}	Width of the teeth on the central rod
Release mechanism	
ϕ	The angle between the origin and lower mounting point of the release system springs
δ	The gripper mounting rotation angle around the z-axis
ψ	The gripper mounting rotation angle around the y-axis
ζ	Angle between the gripper mounting and gripper base
η	Critical rotation angle of the gripper base with respect to the gripper mounting at which release occurs
A, B, C, D	Release system springs mounting points
x_0, x_1, x_2	Magnitude of x-coordinates of the release system springs mounting points
y_0, y_1, y_2	Magnitude of y-coordinates of the release system springs mounting points
O	Origin of the coordinate system chosen in the point of rotation
k_{r}	The spring constant of the release system springs
W_{p}	The weight of the payload
W_{g}	The weight of the gripper
l_{g}	The distance between the origin and the center of gravity
l_{p}	The distance between the origin and payload
l_{s}	The distance between the origin and the spring mounting point on the gripper base
L	Natural length of the release springs

Where the central rod angle θ_6, initial angular offset of the Fin Ray fingers θ_7, and the angular offset of the linkage base θ_8 are design parameters chosen as 30° 100°, and 41°, respectively. The angle θ_1 was used as input for computing the remaining angles and points and was increased incrementally from 15.5° to 33.3°, corresponding to the initial configuration, and the ultimate configuration at which bar ce aligns with bar de, respectively. The resulting workspace is illustrated in Fig. 2(c). Over the entire workspace, the Fin Ray finger angle α ranges from 100° to 56.2°, and the gripper opening l_{f} (see Fig. 2(b)) ranges from 63.3 mm to 6.15 mm.

Although the compliant linkage can also be equipped with rigid gripper fingers, Fin Ray fingers were deployed throughout this work (see Fig. 2(b)) . Fin Ray fingers are triangular in shape with several crossbeams connecting two sides of the triangle such that the fingers bend towards an applied load [20]. As a result, Fin Ray fingers can passively enclose an object and thus do not solely rely on friction grasping. Therefore, the applied normal forces required to hold an object are reduced. Additionally, the contact area between the gripper fingers and the object is increased owing to the compliance of the Fin Ray fingers, thus reducing the pressure being applied to an object.

The rigid central rod demonstrated in Fig. 2(d-i) is suitable for picking up tall objects. However, for shorter objects, the tip of the Fin Ray fingers will collide with the floor before the object makes contact with the central rod to activate the compliant linkage, thus resulting in a failed grasp. To address this issue, the central rod can be equipped with a structure with a nonlinear stiffness characteristic, as shown in Fig. 2(d-ii). Here, the structure's stiffness is designed to be sufficiently high for activating the compliant linkage, but the force applied to the object by the structure does not further increase as it is pushed further onto the object. The force plateau can be tuned by modifying the thickness of the structure.

IEEE Robotics and Automation Letters (RA-L) paper, presented at ICRA 2026, Vienna, Austria. Cite as RA-L paper.

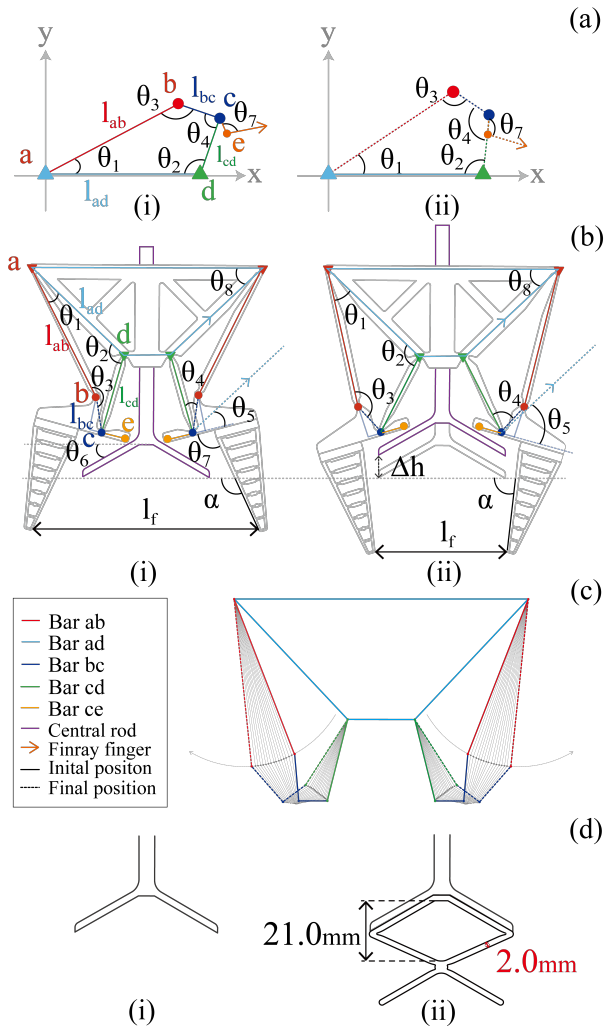

Fig. 2. Illustration of the passive gripper linkage, Fin Ray fingers, and central rod tip: (a) Isolated linkage in its initial (i) and ultimate (ii) configuration, (b) Gripper with linkage, central rod, and Fin Ray fingers, (c) linkage workspace, and (d) rigid central rod tip (i) and compliant central rod tip (ii).

B. Locking mechanism

A linear ratchet mechanism allows the central rod to move upwards through the main body of the gripper, while preventing any downwards movement of the central rod (see Fig. 3). This ensures that the forces applied by the Fin Ray fingers onto the object are maintained when the object is lifted from the ground. The teeth of the gear racks are integrated into the central rod, whereas the spring-loaded pawls are integrated into the main body of the gripper. The teeth on the central rod provide fourteen locking positions over the total possible rod displacement of 37.5 mm, providing a locking resolution of 2.5 mm. The force with which the gripper should be pushed onto the object to move the central rod upwards through the ratchet mechanism can be tuned by adjusting the spring stiffness of the pawl springs.

The free body diagrams of the left pawl and the left half of the central rod are illustrated in Fig. 3(d) and Fig. 3(e) respectively. The weights of the pawls and central rod were considered negligible. In order to move the central rod upward, the pawl spring should be compressed by tooth width w_t (see Fig. 3(e)). Given that the spring is uncompressed in its initial state, the force F_s required to move the pawl spring with spring constant k_l can be calculated as:

$$F_s = w_t \cdot k_l \tag{1}$$

The component of the resultant force F_r along the direction of the slider can be calculated as $F_r \cdot \cos\omega$ (see Fig. 3(d)) and should be greater than F_s to move the central rod upwards. The angle ω can be expressed as a function of the angle of the locking pin β and the friction angle γ. Consequently, the minimal force F_r required to move the mechanism can be expressed in terms of F_s, β, and γ as follows:

$$F_r = \frac{F_s}{\cos(90° + \gamma - \beta)} \tag{2}$$

The pushing force required to realize this F_r on both pawls can be found as $F_p = 2 \cdot F_r \cdot \cos\sigma$ (see Fig. 3(e)), where σ can also be expressed in terms of β and γ, such that:

$$F_p = 2 \cdot F_r \cdot \cos(\beta - \gamma) \tag{3}$$

Finally, equations 1-3 can be combined to:

$$F_p = 2 \cdot w_t \cdot k_l \cdot \frac{\cos(\beta - \gamma)}{\cos(90° + \gamma - \beta)} \tag{4}$$

Here w_t, β, and k_l are design parameters which were chosen as 1.5 mm, 45°, and 166.7 N/m respectively. Friction angle γ can be calculated as $\arctan(\mu)$, where the friction coefficient μ was experimentally determined to be 0.13 (see Section III).

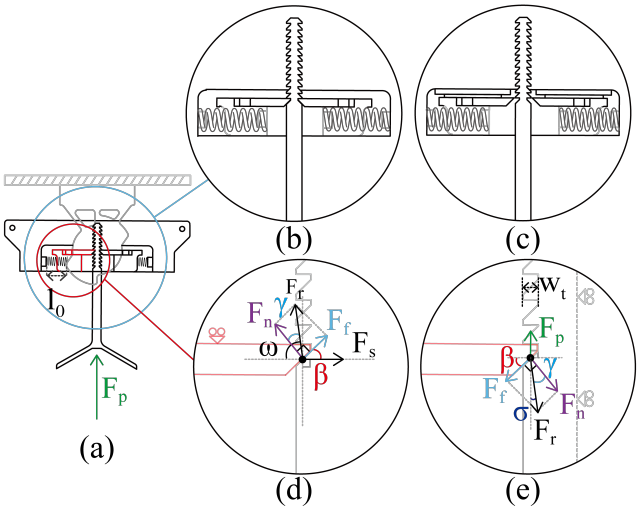

Fig. 3. (a) Illustration of the locking mechanism of the gripper, (b) the mechanism locks the central rod when no force or a pulling force is applied to the central rod, (c) a sufficiently high pushing force on the central rod compresses the pawl springs by w_t and allows the central rod to move upwards, (d) Free body diagram of the left pawl, and (e) Free body diagram of the left half of the central rod

C. Release mechanism

The object can be released using gravitational forces by rotating the gripper base to the release-orientation. This causes the pawls to move along an asymmetric wheel profile (see

IEEE Robotics and Automation Letters (RA-L) paper, presented at ICRA 2026, Vienna, Austria. Cite as RA-L paper.

Fig. 4) until the critical rotation angle of the gripper base with respect to the gripper mounting η is reached, which corresponds to a compression of the pawl springs by w_t. The asymmetry of the profile ensures that the release can only occur when rotating counterclockwise such that the external system (e.g. a robot arm) maintains sufficient DOFs for maneuvering the object in space during transport.

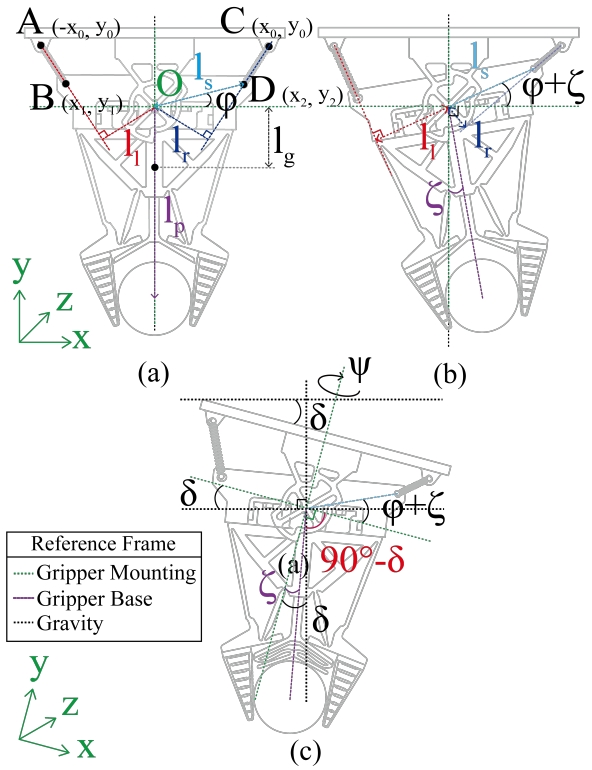

Fig. 4. Annotated illustration of the gripper release mechanism. (a) Gripper mounting rotation angle δ is $0°$ and the angle between the gripper base and mounting ζ is $0°$. (b) $\delta = 0°$ and ζ is equal to the critical rotation angle η at which release occurs. (c) $\delta > 0°$ and $\zeta = \eta$.

An extension spring is placed between the gripper base and mounting on each side of the gripper, as illustrated in Fig. 4. These extension springs provide stability to the system when pressing the central rod on an object for grasping. Moreover, the spring constant k_r of the two springs can be tuned to the weight of the payload to control the gripper mounting rotation angle δ at which the object is released. This can be modeled by considering the moments around rotation point O, as illustrated in Fig. 4(a). It was assumed that the gripper is rotated in a quasi-static manner, and that the moment of the friction caused by the pawl acting on the asymmetric wheel is negligible. For small counterclockwise rotations, the left spring is extended, whereas the right spring is compressed. Therefore, for $\delta - \zeta \in (0, 90°)$ and $\psi(-90, 90)$:

$$\tau_0 + \tau_1 = \tau_2 \tag{5}$$

Where ζ is the angle between the gripper base and mounting (see Fig. 4(b)), ψ is the rotation of the gripper mounting around the y-axis, τ_0 is the moment of the the gripper and payload gravitational force, τ_1 is the moment of the left spring force, and τ_2 is the moment of the right spring force. τ_0 can be divided into the moment of the weight of the gripper and the moment of the payload when the gripper base is static, if the gripper base is rotated at an angle δ, the rotation angle of the gripper with respect to the direction of gravity can be expressed as $\delta - \zeta$ (see Fig. 4(c)), such that τ_0 can be calculated as:

$$\tau_0 = (W_\mathrm{p} \cdot l_\mathrm{p} \cdot \sin(\delta - \zeta) + W_\mathrm{g} \cdot l_\mathrm{g} \cdot \sin(\delta - \zeta)) \cdot \cos\psi \tag{6}$$

Where W_p and W_g are the weight of the payload and gripper respectively, and l_p and l_g their corresponding moment arm distances (see Fig. 4(a)). To find the moments of the two springs of the releasing mechanism, the perpendicular distances between the spring forces and center of rotation need to be calculated. The mounting points of the left and right spring on the robot arm mounting are fixed design parameters and defined as point $A(-x_0, y_0)$ and $C(x_0, y_0)$ respectively. Next, the coordinates of the mounting points of the left and right spring on the gripper are defined as point $B(x_1, y_1)$ and point $D(x_2, y_2)$ respectively (see Fig. 4(a)). Their xy-coordinates can be expressed as:

$$x_1 = -l_\mathrm{s} \cdot \cos(\phi - \zeta) \qquad y_1 = l_\mathrm{s} \cdot \sin(\phi - \zeta)$$
$$x_2 = l_\mathrm{s} \cdot \cos(\phi + \zeta) \qquad y_2 = l_\mathrm{s} \cdot \sin(\phi + \zeta)$$

Where angle ϕ and distance l_s are design parameters illustrated in Fig. 4(a).

To calculate the moment arms of the forces exerted by the springs, we find the equations of the lines moving through point A and B, and C and D, and subsequently calculate the shortest distance between these lines and the origin O as:

$$l_\mathrm{l} = \frac{|x_0 \cdot y_1 + x_1 \cdot y_0|}{\sqrt{(x_0 - x_1)^2 + (y_0 - y_1)^2}} \tag{7}$$

$$l_\mathrm{r} = \frac{|x_0 \cdot y_2 + x_2 \cdot y_0|}{\sqrt{(x_0 - x_2)^2 + (y_0 - y_2)^2}} \tag{8}$$

Next, Hooke's law can be used to find the forces generated by the two springs and multiplied by the arms l_l and l_r to calculate the moments τ_1 and τ_2 respectively:

$$\tau_1 = k_\mathrm{r} \cdot \left| \sqrt{(x_0 - x_1)^2 + (y_0 - y_1)^2} - L \right| \cdot l_l \tag{9}$$

$$\tau_2 = k_\mathrm{r} \cdot \left| \sqrt{(x_0 - x_2)^2 + (y_0 - y_2)^2} - L \right| \cdot l_r \tag{10}$$

Where L is the natural length of the spring. By combining the equations 7-10, τ_1 and τ_2 can be expressed as:

$$\tau_1 = k_\mathrm{r} \cdot |x_0 \cdot y_1 + x_1 \cdot y_0| \cdot \left(1 - \frac{L}{\sqrt{(x_0 - x_1)^2 + (y_0 - y_1)^2}}\right) \tag{11}$$

$$\tau_2 = k_\mathrm{r} \cdot |x_0 \cdot y_2 + x_2 \cdot y_0| \cdot \left(1 - \frac{L}{\sqrt{(x_0 - x_2)^2 + (y_0 - y_2)^2}}\right) \tag{12}$$

By substituting equation 6, 11, and 12 into equation 5, the relationship between the payload and spring constant can be obtained. Here, $\eta = 14°$, $\phi \approx 14.57°$, $l_\mathrm{p} = 0.07$ m, $l_\mathrm{s} \approx$

IEEE Robotics and Automation Letters (RA-L) paper, presented at ICRA 2026, Vienna, Austria. Cite as RA-L paper.

0.052 m , $W_g \approx 0.124$ kg, $l_g \approx 0.035$ m, l_p is estimated as 0.070 m, and L is 0.03 m corresponding to no pre-extension or pre-compression of the spring. The model can be used to select suitable springs for a given payload and desired robot arm rotation angles δ and ψ at which object release should occur. Figure 5 presents the relationship between the four parameters. As the smallest value of δ at which release occurs is always at $\psi = 0$, keeping δ below this value will guarantee retention of the object regardless of ψ.

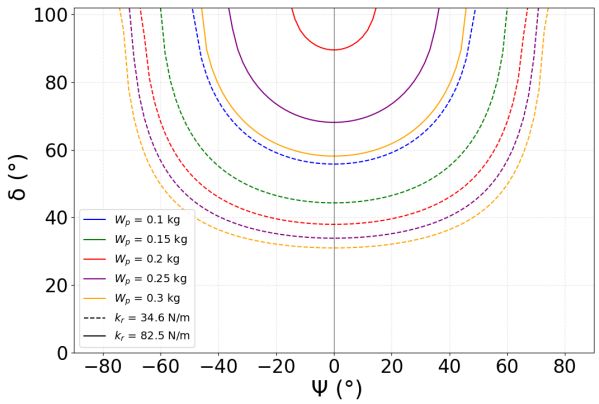

Fig. 5. Relationship between the spring constant of the release mechanism springs k_r, gripper payload W_p, and gripper mounting rotation angles δ and ψ at which release occurs.

III. MATERIALS AND METHODS

A. Gripper fabrication

An exploded view of the passive gripper is shown in Fig. 6. Most parts of the gripper are fabricated by Fused Deposition Modeling (FDM). The robot arm mounting, the gripper base, the asymmetric wheels, the pawls, and the central rod is printed using polylactic acid (PLA) filament (Bambu PLA basic), whereas the Fin Ray fingers are printed using thermoplastic polyurethane (TPU) with a shore hardness of 95A (eSUN eTPU 95-A). Taking inspiration from the fabrication of the PaTS-Wheel compliant linkage [21], the compliant linkage is fabricated by multi-material FDM using PLA to realize rigid links and TPU to realize compliant joints as shown in the inset of Fig. 6. Bonding between the PLA and TPU is achieved through mechanical interlocking, deploying the algorithms described by Kuipers et al. [22]. A mechanical bearing is embedded in the gripper base at the gripper rotation point to ensure stable performance and a high payload capacity. The pawls are attached to sliders to ensure smooth motion of the pawls with minimal friction. The gripper including the mounting has a total weight of 182 g, height of 171 mm, width of 160 mm, and depth of 63 mm. The gripper is built in a modular and scalable way, allowing for easy replacement of different gripper subsystems such as the linkage, central rod, springs, and Fin Ray fingers. By customizing the design parameters and components of the gripper, the design can be modified to suit different user scenarios and needs. For example, additional linkages could be added to both sides of the gripper to increase the number of gripper fingers.

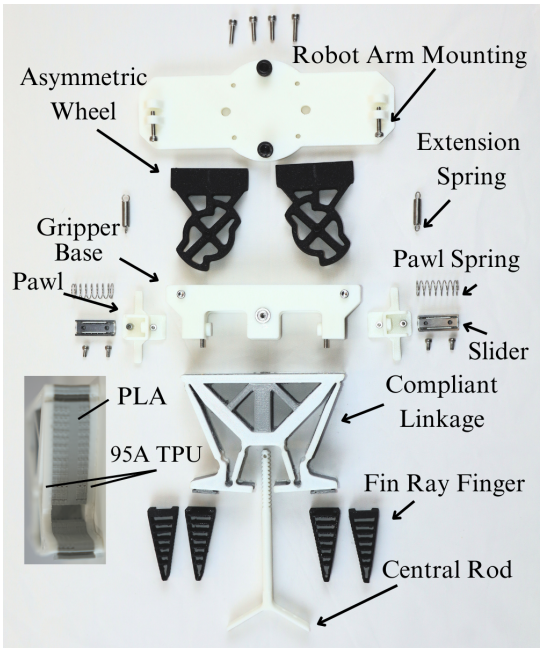

Fig. 6. Annotated overview of the gripper components. Inset: side view of the compliant linkage fabricated using multi-material fused deposition modeling.

B. Experimental setup

Several experiments were performed to verify the models presented in Section II. First, the kinematics of the linkage were evaluated by pushing the central rod up by 2.5 mm (one tooth) at a time and measuring the corresponding Fin Ray finger angle α and gripper opening l_f. Second, the push force required to move the compliant linkage in absence of the locking mechanism and central rod modules was characterized using the measurement setup shown in Fig. 7(b). Next, the compliant central rod tip was characterized using the measurement setup shown in Fig. 7(c). Fourth, the friction coefficient for the PLA pawls and PLA teeth was determined using the measurement setup shown in Fig. 7(d). Here the printing orientations of the sample surfaces were matching the printing orientations of the pawls and teeth to account for the staircase effect in FDM 3D printing. Fifth, the push force required to push the central rod through the locking mechanism in the absence of the compliant linkage was measured using the measurement setup shown in Fig. 7(e). Finally, an experiment was performed to verify the release mechanism model. For a range of different payloads and several springs with different spring constants, the gripper mounting was rotated in counter-clockwise direction in a quasi-static manner until the critical rotation angle η was reached. The gripper mounting rotation angle δ at which release occurred was noted, while gripper mounting rotation angle ψ was kept constant at 0°.

To evaluate the overall adaptive prehension, retention, and release performance of the gripper, the gripper was mounted on a robot arm (see Fig. 7(a)) and used to pick up objects of different sizes, shapes, weights, and surface structures. Next, the compression force and lowering distance of the gripper required for prehension was characterized by picking up a lemon placed on an electronic balance. Note that a small

IEEE Robotics and Automation Letters (RA-L) paper, presented at ICRA 2026, Vienna, Austria. Cite as RA-L paper.

tubular offset was placed in between the balance and the lemon to prevent the Fin Ray fingers from touching the scale during prehension (see Fig. 7(a)). The gripper was moved downwards with decrements of 5 mm and the compression force was noted. After that, the gripper was lifted to see whether it could successfully hold the lemon. Upon reaching the depth at which the gripper could consistently hold the object, the gripper was moved upwards with increments of 2 mm until at least one of the attempts resulted in a failed grasp. Five attempts were made at each depth. This experiment was conducted for both the rigid central rod tip as the compliant central rod tip. Finally, a repeatability test was performed, where the apple was picked up 50 times.

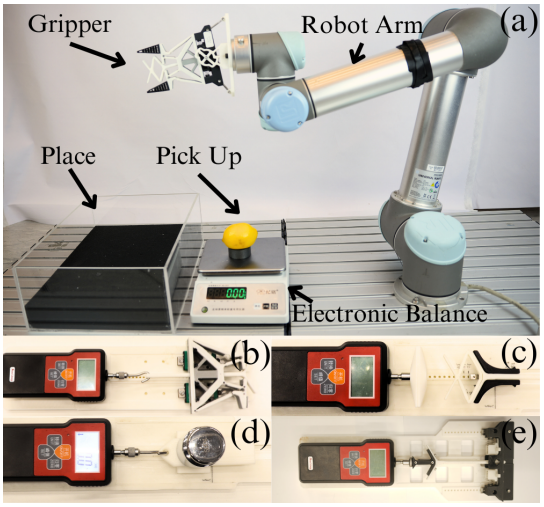

Fig. 7. Experimental setup for characterization and performance evaluation: (a) Pick and place and compression force experiment, (b) compliant linkage push force with displacement of central rod experiment, (c) compliant central rod tip push force characterization, (d) experiment for determining the friction coefficient between PLA parts, and (e) locking mechanism push force with displacement of central rod experiment.

IV. RESULTS

A. Linkage kinematics

The results of the characterization of the linkage are shown in Fig. 8(a). It can be found that the experimental characterization is in good agreement with the model, although the maximum central rod displacement Δh (see Fig. 2(b-ii)) of 17.5 mm is slightly lower than the modeled ultimate position of the linkage due to the thickness of its bars. It should be noted that the central rod can be pushed upwards beyond 17.5 mm to close the gripper slightly further, but this results in damage to the compliant linkage. The Fin Ray finger angle α (see Fig. 2(b)) ranges from 100° to 64.2° and the gripper opening l_f (see Fig. 2(b)) ranges from 70.5 mm to 16.5 mm over the total vertical displacement of the central rod.

B. Pushing force for gripper closure

The total push force required to close the gripper before the Fin Ray fingers make contact with the object is the sum of (i) the push force required to rotate around the compliant joints, (ii) the push force required to compress the compliant central rod tip, and (iii) the force required to move the central rod upwards through the locking mechanism. First, experiments were conducted to measure these forces in an isolated manner. The push force required to rotate the compliant joints in absence of the locking mechanism was measured using the setup shown in Fig. 7(b) and the results are shown in Fig. 8(a). The push force required to compress the compliant central

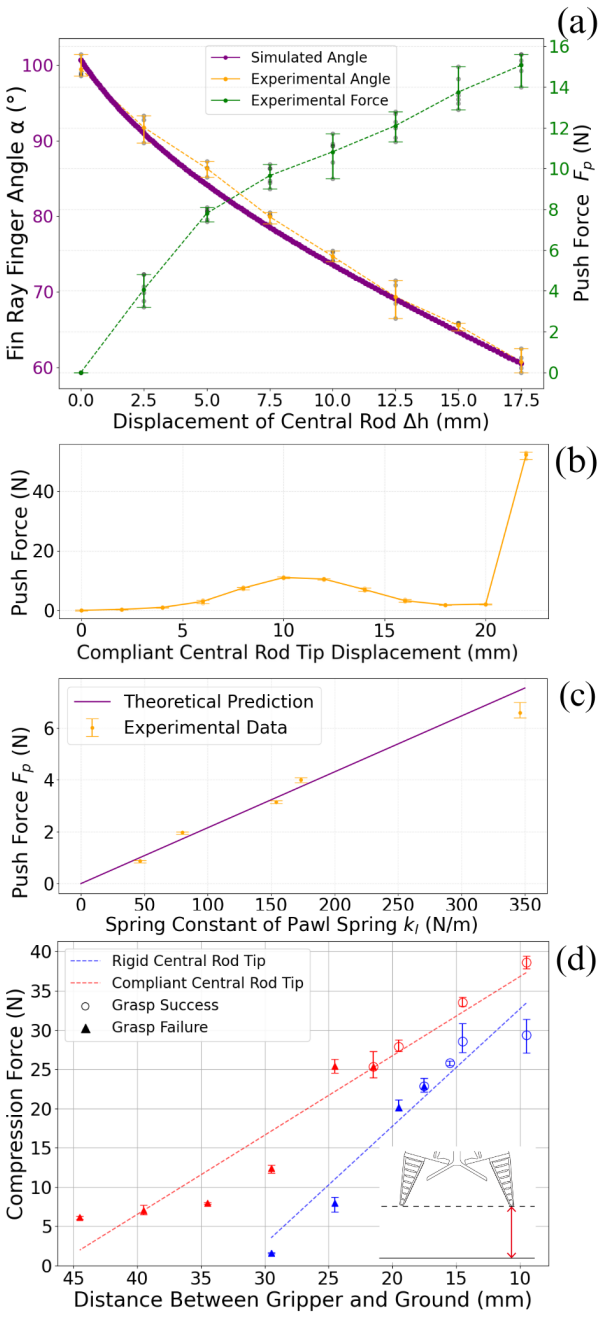

Fig. 8. (a) Relationship between the vertical displacement of the rod Δh (x-axis) and Fin Ray finger angle α (left y-axis) and required push force on the central rod (right y-axis), (b) Relationship between push force and displacement of the compliant central rod tip, (c) Relationship between the push force on the central and the spring constant of the pawl springs, and (d) Compression force applied to the payload at varying distance between the gripper and the ground (see inset) for both the compliant central rod tip as the rigid central rod tip. Triangles indicate that the gripper was unable to pick up the object at this indentation, whereas circles indicate successful pick up.

IEEE Robotics and Automation Letters (RA-L) paper, presented at ICRA 2026, Vienna, Austria. Cite as RA-L paper.

rod tip was measured using the setup shown in Fig. 7(c) and the result is shown in Fig. 8(b). It can be found that there is a force plateau at 11.0 N. Comparing this value to the push force required to move the compliant linkage (see Fig. 8(b)), it becomes apparent that the compliant central rod tip can successfully activate the compliant linkage before the compliant central rod tip is getting fully compressed. The steep increase in push force between 20 mm and 22 mm of compliant central rod tip displacement can be explained by the full collapse of the compliant central rod tip structure which had an initial gap of 21 mm (see Fig. 2(d-ii)).

Next, the force required to push the central rod through the locking mechanism in the absence of the compliant linkage was measured using the setup setup shown in Fig. 7(e). The results are reported in Fig. 8(c). The experimental results are in good agreement with the locking mechanism model.

Finally, the compression force exerted onto a lemon was tested using the measurement setup shown in Fig. 7(a) and the results are shown in Fig. 8(d). For both the rigid central rod tip and the compliant central rod tip, the gripper could consistently pick up the lemon at compression forces below 30 N. For reference, the maximum tolerable compression force on apples was demonstrated to be around 40 N [23]. The results also show that the compliant central rod tip was able to consistently pick up the lemon at a slightly higher distance between the gripper and the ground (see inset Fig. 8(d)) of 21.5 mm, but also at a slightly higher compression force (27.9 N) than the rigid central rod tip (17.5 mm and 25.8 N respectively). This is further highlighted in the supplementary video.

C. Release mechanism model

The results of the experiment for validating the release mechanism model presented in subsection II-C are shown in Fig. 9. The angle δ at which the gripper releases the object (at $\psi = 0$) was measured for four different release mechanism spring configurations and six different payloads. The results are in reasonable agreements with the model. As the compression of the pawl springs by tooth width w_t occurs over a small change in angle between the gripper base and gripper mounting ζ, the exact gripper mounting rotation angle at which release occurs is sensitive to small manufacturing and assembly inaccuracies in the release mechanism. The supplementary video demonstrates the release mechanism for different objects and release mechanism spring configurations when the gripper is mounted on a robot arm. The video also highlights the change in release angle δ at different values of ψ, as modeled in Fig. 9.

D. Adaptive grasping performance

The grasping performance was evaluated on a range of objects using the measurement setup shown in Fig. 7(a) and is highlighted in the supplementary video. The gripper was able to successfully pick up lemons, apples, corn cobs, carrots, a whiteboard eraser, a roll of tape, and a metallic container, highlighting the gripper's ability to adapt to objects of various shapes, weights, and sizes. The fundamental grasping limitations are shown in Fig. 10. Objects that are too low cannot be picked up as the Fin Ray fingers will touch the ground before the central rod is activated (see Fig. 10(a)). The compliant central rod tip can be equipped to address this problem. Second, the gripper cannot pick up objects that are too slender, as the gripper opening l_f is still too large at the maximum displacement of the central rod Δh (see Fig. 10(b)). Third, the gripper struggles to pick up objects with a tapered shape, as the normal forces exerted by the Fin Ray fingers will generate a downwards force component on the object (see Fig. 10(c)). Fourth, the gripper cannot pick up objects that are too large for the Fin Ray fingers to enclose the object (see Fig. 10(d)). Fifth, the gripper cannot pick up unstable shapes that cause the gripper base to rotate around the rotation point when the gripper is being pressed onto the object (see Fig. 10(e)). Finally, the gripper is unable to pick up objects that are too soft, such that the object compresses instead of pushing the central rod upwards (see Fig. 10(f)). Examples of these failure modes can be found in the supplementary video.

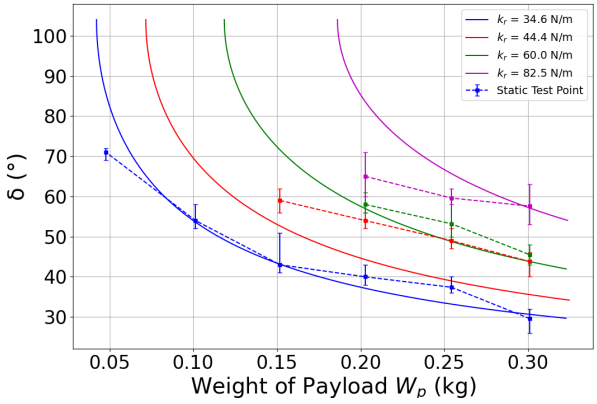

Fig. 9. Relationship between the weight of the payload W_p and gripper mounting rotation angle δ at which release occurs for release mechanism spring configurations with k_r equal to 34.6, 44.4, 60.0, and 82.5. The model prediction is shown as a solid line, whereas the quasi-static experiments are shown as squares connected by dashed lines.

E. Object retention performance

An overview of the prehension, retention, and release of an apple with the passive gripper is shown in Fig. 11. The gripper firmly holds the object in a wide range of orientations (Fig. 11(d-i)), including one of its fully sidewards orientations (Fig. 11(g)). Hereby, the robot arm is provided with sufficient degrees of freedom to maneuver the object to the desired position and orientation, including its upside-down orientation. Only when the gripper is maneuvered in the opposite sidewards orientation will the object be released (Fig. 11(j)). The object retention performance is further highlighted in the supplementary video.

F. Repeatability test

A repeatability test was conducted to evaluate the stability of the prehension, retention and release mechanisms. Apples with a weight of 110.5 ± 12.1 grams were picked up 50 times with a 100% success rate, demonstrating reliable performance

IEEE Robotics and Automation Letters (RA-L) paper, presented at ICRA 2026, Vienna, Austria. Cite as RA-L paper.

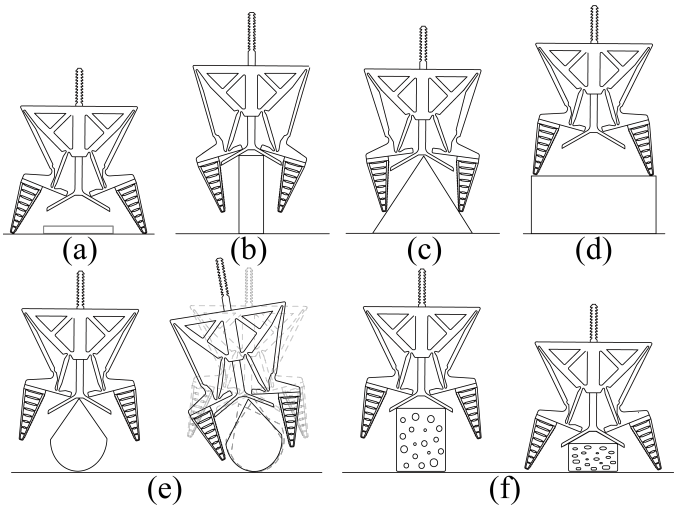

Fig. 10. Limitations of the passive adaptive gripper in grasping (a) objects with low heights, (b) slender objects, (c) tapered objects, (d) large objects, (e) unstable objects, and (f) soft objects.

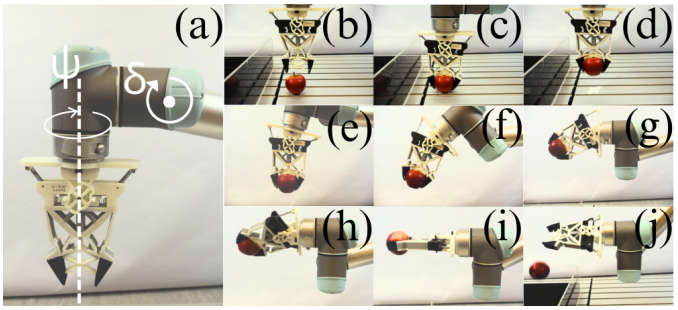

Fig. 11. Object prehension, retention, and release. The gripper firmly holds the object in a wide range of orientations (d-i), including one of its fully sidewards orientations (g). Only when the gripper is maneuvered in the opposite sidewards orientation will the object be released (j).

of the multi-material linkage with compliant joints and locking and release mechanism. The gripper repeatability experiments are further highlighted in the supplementary video.

V. CONCLUSION

This article presented a mechanically intelligent gripper capable of passive adaptive object prehension, retention, and contactless release without the need for any actuator or power source besides the robot arm. The absence of actuators, electronics, and a tether or embedded power source make the presented adaptive gripper a promising technology for challenging environments where low energy consumption and robustness to dust and water are critical. Future work will focus on the integration of the gripper on a UUV for underwater manipulation tasks.

REFERENCES

[1] H. Liu, K. Wu, P. Meusel, N. Seitz, G. Hirzinger, M. Jin, Y. Liu, S. Fan, T. Lan, and Z. Chen, "Multisensory five-finger dexterous hand: The dlr/hit hand ii," in *2008 IEEE/RSJ International Conference on Intelligent Robots and Systems*, 2008, pp. 3692–3697.

[2] J. Shintake, V. Cacucciolo, D. Floreano, and H. Shea, "Soft robotic grippers," *Advanced Materials*, vol. 30, no. 29, p. 1707035, 2018.

[3] D. Yoon and K. Kim, "Fully passive robotic finger for human-inspired adaptive grasping in environmental constraints," *IEEE/ASME Transactions on Mechatronics*, vol. 27, no. 5, pp. 3841–3852, 2022.

[4] S. B. Backus and A. M. Dollar, "An adaptive three-fingered prismatic gripper with passive rotational joints," *IEEE Robotics and Automation Letters*, vol. 1, no. 2, pp. 668–675, 2016.

[5] C. Meijneke, G. A. Kragten, and M. Wisse, "Design and performance assessment of an underactuated hand for industrial applications," *Mechanical Sciences*, vol. 2, no. 1, pp. 9–15, 2011.

[6] W. Townsend, "The barretthand grasper – programmably flexible part handling and assembly," *Industrial Robot: An International Journal*, vol. 27, pp. 181–188, 1 2000.

[7] Y. Zhai, A. D. Boer, J. Yan, B. Shih, M. Faber, J. Speros, R. Gupta, and M. T. Tolley, "Desktop fabrication of monolithic soft robotic devices with embedded fluidic control circuits," *Science Robotics*, vol. 8, no. 79, p. eadg3792, 2023.

[8] P. Kappel, L. Kürner, T. Speck, and F. Tauber, "A pneumatic bending actuator system inspired by the avian tendon locking mechanism," in *Biomimetic and Biohybrid Systems*. Cham: Springer Nature Switzerland, 2023, pp. 84–100.

[9] W. Crooks, S. Rozen-Levy, B. Trimmer, C. Rogers, and W. Messner, "Passive gripper inspired by manduca sexta and the fin ray® effect," *International Journal of Advanced Robotic Systems*, vol. 14, no. 4, p. 1729881417721155, 2017.

[10] J. Hsu, E. Yoshida, K. Harada, and A. Kheddar, "Self-locking underactuated mechanism for robotic gripper," in *2017 IEEE International Conference on Advanced Intelligent Mechatronics (AIM)*, 2017, pp. 620–627.

[11] X.-Y. Guo, W.-B. Li, Q.-H. Gao, H. Yan, Y.-Q. Fei, and W.-M. Zhang, "Self-locking mechanism for variable stiffness rigid–soft gripper," *Smart Materials and Structures*, vol. 29, no. 3, p. 035033, feb 2020.

[12] Y. Li, Y. Chen, Y. Yang, and Y. Wei, "Passive particle jamming and its stiffening of soft robotic grippers," *IEEE Transactions on Robotics*, vol. 33, no. 2, pp. 446–455, 2017.

[13] M. Plooij, G. Mathijssen, P. Cherelle, D. Lefeber, and B. Vanderborght, "Lock your robot: A review of locking devices in robotics," *IEEE Robotics Automation Magazine*, vol. 22, no. 1, pp. 106–117, 2015.

[14] H. Hsiao, J. Sun, H. Zhang, and J. Zhao, "A mechanically intelligent and passive gripper for aerial perching and grasping," *IEEE/ASME Transactions on Mechatronics*, vol. 27, no. 6, pp. 5243–5253, 2022.

[15] H. Hsiao, F. Wu, J. Sun, and J. Zhao, "A novel passive mechanism for flying robots to perch onto surfaces," in *2022 International Conference on Robotics and Automation (ICRA)*, 2022, pp. 1183–1189.

[16] S. M. Lee, J. Liu, J. L. Chien, W. H. Ng, M. Lim, and S. Foong, "Rapid resistography with passive overhead-perching mechanism in an unmanned aerial system for wood structure inspection," in *2024 IEEE International Conference on Robotics and Automation (ICRA)*, 2024, pp. 1554–1560.

[17] K. Nagaoka, H. Minote, K. Maruya, Y. Shirai, K. Yoshida, T. Hakamada, H. Sawada, and T. Kubota, "Passive spine gripper for free-climbing robot in extreme terrain," *IEEE Robotics and Automation Letters*, vol. 3, no. 3, pp. 1765–1770, 2018.

[18] Q. Qi, C. Xiang, V. A. Ho, and J. Rossiter, "A sea-anemone-inspired, multifunctional, bistable gripper," *Soft Robotics*, vol. 9, no. 6, pp. 1040–1051, 2022.

[19] I. Nate, Z. Wang, and S. Hirai, "Passive robotic gripper using a contact-based locking mechanism," in *2023 IEEE International Conference on Robotics and Automation (ICRA)*, 2023, pp. 10 303–10 309.

[20] W. Crooks, G. Vukasin, M. O'Sullivan, W. Messner, and C. Rogers, "Fin ray® effect inspired soft robotic gripper: From the robosoft grand challenge toward optimization," *Frontiers in Robotics and AI*, vol. Volume 3 - 2016, 2016.

[21] T. Godden, B. W. Mulvey, E. Redgrave, and T. Nanayakkara, "Patswheel: A passively-transformable single-part wheel for mobile robot navigation on unstructured terrain," *IEEE Robotics and Automation Letters*, vol. 9, no. 6, pp. 5512–5519, 2024.

[22] T. Kuipers, R. Su, J. Wu, and C. C. Wang, "ITIL: Interlaced topologically interlocking lattice for continuous dual-material extrusion," *Additive Manufacturing*, vol. 50, p. 102495, 2022.

[23] J. Zhu, D. Zhu, L. Wang, K. Xue, J. Liao, and S. Zhang, "Effects of compression damage on mechanical behavior and quality attributes of apple fruit," *Food Science and Technology Research*, vol. 28, no. 1, pp. 53–65, 2022.